ORIGINAL ARTICLE
DOI: 10.4274/tjps.galenos.2024.49768

IN SILICO EVALUATION OF H1-ANTIHISTAMINE DRUGS AS POTENTIAL INHIBITORS OF SARS-COV-2 RNA-DEPENDENT RNA POLYMERASE: A REPURPOSING STUDY FOR COVID-19 THERAPY

Hamdan et al. Repurposing of H1-Antihistamines as SARS-CoV-2 Inhibitors

Mazın Hamdan[1], Necla Kulabaş[2], İlkay Küçükgüzel[3]

[1]Department of Pharmaceutical Chemistry, Institute of Health Sciences, Marmara University, İstanbul, Turkey
[2]Department of Pharmaceutical Chemistry, Faculty of Pharmacy, Marmara University, Istanbul, Turkey
[3]Department of Pharmaceutical Chemistry, Faculty of Pharmacy, Fenerbahçe University, İstanbul, Turkey

Corresponding Author Information
İlkay Küçükgüzel
ilkay.kucukguzel@fbu.edu.tr
+90 532 795 29 13
https://orcid.org/0000-0002-7188-1859
31.05.2024
23.06.2024
25.06.2024

Abstract
INTRODUCTION:
SARS-CoV-2, from the Coronaviridae family, is the seventh known type of coronavirus to infect humans and causes acute respiratory syndrome. Rapidly spreading worldwide, the virus emerged in Wuhan, China, in December 2019, leading to an ongoing pandemic with more than 775 million confirmed cases and over 7 million deaths (as of May 5th 2024), according to World Health Organization data. Although vaccination efforts have been undertaken, the lack of an FDA-approved antiviral agent aimed at curing the disease has made the drug repurposing a key approach for urgent intervention in the COVID-19 pandemic. This study investigates the potential of H1-antihistamines as antiviral agents against SARS-CoV-2, the virus that causes COVID-19. We targeted the main replicase/transcriptase complex (RTC) of the virus, specifically nonstructural protein 12 (nsp12), which is essential for viral RNA synthesis.
METHODS:
Using molecular docking techniques, we explored the interactions between H1-antihistamines and RNA-dependent RNA polymerase (RdRp), a key enzyme in viral replication. The three-dimensional structure of 37 H1-antihistamine molecules was drawn and their energies were minimized using Spartan 0.4. Subsequently, we conducted a docking study with Autodock Vina to assess the binding affinity of these molecules to the target site. The docking scores and conformations were then visualized using Discovery Studio.
RESULTS:
The results examined showed that the docking scores of the H1-antihistamines were between -5.0 and -8.3 kcal/mol. The findings suggest that among all analyzed drugs, bilastine, fexofenadine, montelukast, zafirlukast, mizolastine, rupatadine can bind with the best binding energy (< -7.0 kcal/mol) and inhibit RdRp, potentially halting the replication of the virus.
DISCUSSION AND CONCLUSION:
This study highlights the promise of H1-antihistamines in combating COVID-19 and underscores the value of computational approaches in rapid drug discovery and repurposing efforts. Finally, experimental studies are required to measure the potency of H1-antihistamines before their clinical use against COVID-19 as RdRp inhibitors.
Keywords: SARS-CoV-2; RNA-dependent RNA polymerase; molecular docking; H1-antihistamines; drug repurposing

INTRODUCTION

uncorrected proof

Infectious diseases caused by various microorganisms, including viruses, bacteria, fungi, and parasites, continue to be one of the most significant public health issues [https://www.emro.who.int/health-topics/infectious-diseases/index.html, (accessed on May. 21, 2024)][1]. Among the most serious infection categories, RNA virus infections significantly contribute to the global index of mortality and morbidity related to viral infections. Chronic disease due to persistent RNA virus infections represents a significant public health concern [2]. The global population continues to combat many infectious diseases caused by these pathogens, some of which have become epidemics or pandemics [3]. The World Health Organization (WHO) declared coronavirus disease 2019 (COVID-19), caused by the severe acute respiratory syndrome coronavirus-2 (SARS-CoV-2), a global public health emergency on March 11, 2020, due to its extensive impact. By early May 2024, more than 7 million deaths and over 775 million infected cases had been reported [https://www.who.int/emergencies/diseases/novel-coronavirus-2019, (accessed on May. 21, 2024)][4]. The first known case of SARS-CoV-2 was identified in Wuhan in China, and it is an RNA virus from the *Coronaviridae* family that rapidly led to a global pandemic due to its high transmissibility [5-7]. The Beta, Gamma, Delta, and Omicron variants arising from viral mutations of SARS-CoV-2 have also caused significant damage to the world economy. Repurposed drugs and vaccines developed to combat the pandemic have played a crucial role in mitigating its impact and restoring socioeconomic stability [8]. Reuse can be achieved through high-efficiency *in vitro* analyses, *in vivo* investigations in animals, and computer-aided drug discovery techniques. Studies on the reuse of many known drugs, including antivirals, antimalarials, H1-antihistamines, antipsychotics and anticancer agents, are available in the literature [9-13]. While known safety profiles of approved drugs have allowed rapid progress in clinical trials, limited success has been achieved in identifying clinically effective small-molecule drugs for COVID-19 treatment [14-16].

H1-Antihistamines are a class of drugs commonly used to treat allergic reactions, such as hay fever, hives, and itching [17]. They work by blocking the action of histamine, a substance in the body that causes allergic symptoms. H1-Antihistamines can be divided into two main types; first-generation and second-generation. First-generation H1-antihistamines, such as diphenhydramine and chlorpheniramine, tend to cause more drowsiness and are often used for short-term relief of symptoms. Second-generation H1-antihistamines, such as loratadine and cetirizine, are less sedating and are preferred for long-term use [18]. Traditionally recognized for their role in mitigating allergic responses by antagonizing histamine receptors, H1-antihistamines have recently garnered attention for their broader pharmacological effects, including potential antiviral properties. This paradigm shift is underpinned by advancements in computational modeling and virtual screening methodologies, enabling us to elucidate the intricate molecular interactions between H1-antihistamines and viral targets.

In a study conducted in 2021, H1-antihistamine agents such as hydroxyzine, azelastine, and diphenhydramine were reported to have *in vitro* antiviral activity against SARS-CoV-2. Moreover, it was reported that hydroxyzine exhibits antiviral activity through the mechanism of Angiotensin Converting Enzyme 2 (ACE-2) inhibition, while azelastine and diphenhydramine compounds exert their effects by binding to the sigma-1 receptor [12]. In another study reported by Ghahremanpour et al., it was detected that azelastine has the potential to inhibit the main protease (MPro) which is structural protein of SARS-CoV-2 [11]. Additionally, it has been reported in the literature that fexofenadine, another H1-antihistamine, has the potential to inhibit the SARS-CoV-2 helicase enzyme [10]. The interactions of H1-antihistamines with antiviral targets reported in the literature are summarized in Figure 1.

Although the body systems they affect, transmission routes and symptoms are different, there are many studies investigating similarities between the non-structural (NS3) proteins of SARS-CoV-2 and hepatitis-C virus (HCV). These studies indicate that these proteins share structural similarities as well as some functional properties. Specifically, NS3 proteins include protease and helicase activities critical in the replication process of both viruses. These similarities could guide the development of potentially effective antiviral agents against NS3 proteins of SARS-CoV-2 and HCV. In a groundbreaking study published in 2014, Haid et. al revealed compelling evidence of the selective inhibition of hepatitis C virus (HCV) infection by hydroxyzine and benztropine. This study, led by esteemed experts in virology, unveiled the remarkable antiviral properties of these two compounds, shedding light on their potential as potent agents against HCV. Through meticulous experimentation and rigorous analysis, the researchers elucidated the mechanism by which hydroxyzine and benztropine exert their inhibitory effects on HCV infection. By selectively targeting key NS3 protein or host cell factors crucial for viral replication, these compounds demonstrated a remarkable ability to disrupt the viral lifecycle, thereby impeding viral propagation and spread. The findings of this study not only underscore the significance of hydroxyzine and benztropine as possible candidates for antiviral therapy against HCV but also pave the way for further exploration of their therapeutic potential in combating other viral infections [19]. Similarly, in a notable study by Zongy et al., it was revealed that chlorcyclizine exerts its antiviral effect against hepatitis C virus (HCV) by targeting the viral envelope glycoprotein. This finding underscores the potential of chlorcyclizine as a promising antiviral agent against HCV infection [20].

uncorrected proof

In the dynamic landscape of drug discovery, the integration of computational techniques has revolutionized the exploration of pharmaceutical interventions [21]. *In silico* studies, which encompass a spectrum of computational methods, have emerged as invaluable tools for accelerating the identification and evaluation of potential drug candidates. In the approach of repurposing known drugs, the primary objective of computational and experimental techniques has been to identify existing drugs that may be effective against SARS-CoV-2.

In RNA viruses like SARS-CoV-2, the RNA-dependent RNA polymerase (RdRp) enzyme creates the machinery required for RNA synthesis and the organized replication and transcription of genomic RNA [22]. After the virus attacks a host cell, the viral genomic RNA is used directly as a template, and the host cell's protein synthesis machinery is utilized for the translation of RdRp [23]. RdRp, is an enzyme crucial for the replication of RNA viruses [24]. It catalyzes the synthesis of RNA from an RNA template, a process essential for the reproduction of RNA viruses like influenza, hepatitis C, and coronaviruses (including SARS-CoV-2). RdRp is a prime target for antiviral drugs aimed at inhibiting viral replication. In the context of the COVID-19 pandemic, drugs like remdesivir have gained attention for their ability to inhibit RdRp and potentially reduce the severity of the disease [25]. The structure of the SARS-CoV-2 RdRp complex comprises a core catalytic unit consisting of an non-structural-protein 12 (nsp12) core, an nsp7-nsp8 (nsp8-1) heterodimer, and an additional nsp8 subunit (nsp8-2) (Figure 2). The nsp12-nsp7-nsp8 complex is identified as the minimal core component for viral RNA replication [26]. A 30 kb SARS-CoV-2 genome contains 14 open reading frames (ORF) that can encode at least 27 proteins [27]. The ORF 1 ab region at the 5´ end consists of a polyprotein and is hydrolyzed to 16 nonstructural proteins nsp 1-16 to form a replicase/transcriptase complex (RTC). The main RTC is RdRp nsp 12 [28]. Nsp-12 has 8 motifs (A to G); **Motif C** (F753-N767) contains the catalytic **motif SDD** (Ser759, Asp760, and Asp761), which is required for metal ion binding [26] and this site is going to be our main target, in this study.

This study lays the groundwork for exploring the rapidly growing field of *in silico* research aimed at uncovering the antiviral potential of H1-antihistamines. By utilizing molecular modeling techniques, we seek to understand the mechanisms behind the potential antiviral effects associated SARS-CoV-2 RdRp enzyme inhibition of these drugs. Moreover, these investigations provide insights into the therapeutic potential of H1-antihistamines against various viral infections, opening new possibilities for drug repurposing and therapeutic development. Although montelukast and zafirlukast are not typically classified as H1-antihistamines, they belong to a class of medications known as leukotriene receptor antagonists (LTRAs). These drugs work by blocking the action of leukotrienes, which are inflammatory substances produced by the body in response to allergens or other triggers. While they are often used to manage asthma and allergic rhinitis, they do not directly target histamine receptors like traditional H1-antihistamines do. However, they can help relieve symptoms associated with allergic reactions, such as inflammation and bronchoconstriction [29]. Since the potential of zafirlukast to inhibit the SARS-CoV-2 helicase enzyme has been reported in the literature [30], in this study, an *in silico* investigation of montelukast and zafirlukast was also conducted.

MATERIALS AND METHODS

System Preparation

Protein Preparation

A recently reported high-resolution X-ray structure of RdRp (2.90 Å) (PDB ID 6M71: https://www.rcsb.org/3d-view/ngl/6m71) [26] was used in this study. After the protein crystal structure was obtained, all water molecules and ions were initially deleted. The protein was then saved in .pdb format and was subsequently converted to pdbqt format using Autodocktools 1.5.7 [31]. Later, the region of Ser759, Asp760, and Asp761 was determined as the location of the grid box (114.52, 114.11,122.91) using Discovery Studio 2021 and Autodocktools 1.5.7.

Preparation of the ligands

All ligands were drawn using Spartan 4.0 and each molecule's energy was also minimized using Spartan 4.0 [32], the conformations with the lowest energy were saved in .pdb format and then converted to.pdbqt format using Autodocktools 1.5.7. Brompheniramine, levocetirizine, montelukast and chlorpheniramine were drawn as their pharmacologically active (*R*) stereoisomers. Cetirizine, dexchlorpheniramine and triprolidine were drawn as their pharmacologically active (*S*) stereoisomers.

Molecular Docking

The determination of the grid box region (114.52, 114.11,122.91) and dimensions (30,30,30 Å) to include Ser759, Asp760, and Asp761 region was made using AutodockTools 1.5.7. and Discovery Studio 2021. Then molecular docking was made using Autodock Vina [33]. Each docking process was repeated at least 3 times to ensure the accuracy of the results. Later on, each molecule docking score and confirmations were visualized using Discovery Studio 2021. Each molecule's binding energy is demonstrated in Figures 3, 4 and 5.

RESULTS

uncorrected proof

In this study, the *in silico* binding potentials of 37 drugs, including FDA-approved H1-antihistamines as well as montelukast and zafirlukast, against the SARS-CoV-2 RdRp enzyme were examined (Figures 3-5). Table 1-7 present comprehensive visual representations of the three-dimensional (3D) and two-dimensional (2D) interactions of the best potential SARS-CoV-2 RdRp inhibitors that bilastine, fexofenadine, montelukast, zafirlukast, mizolastine, rupatadine and terfenadine, respectively.

The docking results indicate that bilastine binds effectively to RdRp, primarily through hydrogen bonds and electrostatic interactions (Table 1). The strong binding energy and specific interactions suggest that bilastine could inhibit the function of RdRp, potentially blocking the replication of the virus. Bilastine shows significant binding affinity against SARS-CoV-2 RdRp enzyme with -7.6 kcal/mol binding energy value in Figure 3. The carboxylic acid group within bilastine forms crucial hydrogen bonds with specific residues of RdRp, illuminating the intricate nature of their molecular interaction. One notable interaction occurs between the carboxylic acid group and Asp761, wherein a hydrogen bond is established with a bond length of 2.26 Å. Additionally, another hydrogen bond detected between this group and Ser814, further emphasizing the nuanced connectivity between bilastine and RdRp, characterized by a bond length of 2.43 Å. Moreover, the ethoxy group present in bilastine contributes significantly to its interaction with RdRp. This group forms hydrogen bonds with Asp623 and Cyc622, underscoring the multifaceted nature of bilastine's engagement with the receptor. The hydrogen bond lengths between the ethoxy group and Asp623 and Cyc622 are measured at 2.25 Å and 2.27 Å, respectively. Beyond hydrogen bonding, electrostatic and pi-cation interactions also play a substantial role in shaping the binding profile of bilastine with RdRp. The benzimidazole moiety within bilastine demonstrates such interactions with key residues of RdRp, namely Arg553 and Lys621. These interactions occur at distances of 4.27 Å and 4.32 Å with Arg553 and at distances of 4.94 Å and 4.78 Å with Lys621, showcasing the diverse array of molecular forces at play in bilastine-RdRp binding. The interactions with critical residues such as Asp761, Ser814, and Arg553 underscore the potential of bilastine as a therapeutic candidate, warranting further investigation.

Our docking study has identified fexofenadine (Table 2), as a potential inhibitor of the SARS-CoV-2 RdRp. The docking results reveal a binding energy of -8.0 kcal/mol, indicating a strong binding affinity. In the context of molecular interactions, the carboxylic acid group of fexofenadine plays a crucial role by establishing significant hydrogen bonds with specific residues of RdRp. Notably, hydrogen bonds are formed with Trp617 and Trp800, with bond lengths of 2.91 Å and 2.76 Å, respectively. Moreover, a particularly strong hydrogen bond is formed with Glu811, with a bond length of 2.02 Å. Beyond hydrogen bonding, fexofenadine exhibits hydrophobic and pi interactions, further enriching its binding profile with RdRp. The phenyl group within fexofenadine engages in hydrophobic and pi interactions with Tyr455 and Arg553, with distances of 5.57 Å and 4.38 Å, respectively. Additionally, multiple interactions with Lys621 are observed, including electrostatic/pi-cation interactions at distances of 4.62 Å and 5.46 Å. Furthermore, a hydrophobic/pi-alkyl interaction is noted with Arg624, with a distance of 3.09 Å. In summary, the comprehensive analysis of hydrogen bonding, hydrophobic, pi, and additional interactions reveals the intricate molecular landscape governing the interaction between fexofenadine and RdRp, offering valuable insights into its potential therapeutic efficacy against viral infections.

Montelukast, with a binding energy of -7.2 kcal/mol, demonstrated a multifaceted binding profile characterized by hydrogen bonding, hydrophobic interactions, and electrostatic contacts (Table 3). Specifically, hydrogen bonds formed between montelukast and key residues Lys798, Trp800, and Asp760 underscored the importance of specific molecular recognition patterns in stabilizing the Montelukast-RdRp complex. Moreover, hydrophobic interactions with Tyr455 and electrostatic interactions with Lys621 provided additional stability to the complex, highlighting the diverse array of interactions contributing to the ligand-receptor binding. Three hydrogen bonds are predicted to form between montelukast's carboxylic acid group and residues Lys798, Trp800, and Asp760 of RdRp. These hydrogen bonds can contribute significantly to the stability of the ligand-receptor complex. The 7-methylquinoline moiety of montelukast participates in many hydrophobic interactions with Tyr455, Arg553, and Lys621 residues of RdRp, which help retain the ligand in the binding pocket.

On the other hand, zafirlukast exhibited a higher binding energy of -8.3 kcal/mol, indicative of stronger binding affinity. The binding profile of zafirlukast was characterized by an extensive network of hydrogen bonds involving residues Cys622, Asp623, Asp760, Asp761, Cys813, and Cys814, predominantly mediated by carbamate and amide functional groups (Table 4). This intricate hydrogen bonding network underscores the specific molecular recognition events driving the formation of the zafirlukast-RdRp complex. Zafirlukast utilizes its carbamate group to form hydrogen bonds with both Cys622 and Asp623, potentially anchoring it within the binding pocket. Additionally, hydrogen bonds are formed between the ligand's nitrogens and key residues Asp760 and Asp761, potentially contributing to directional positioning. Furthermore, the participation of Cys813 and Cys814 through hydrogen bonds with the ligand's amide carbonyl group suggests a role in stabilizing the complex. The presence of a pi-anion

uncorrected proof

interaction between the ligand's benzene sulfonyl group and Asp618 suggests an attractive force that could contribute to the overall binding affinity. Moreover, a pi-sulfur interaction between the same sulfonyl group and Trp800 highlights potential aromatic stacking, which could further enhance the stability of the complex. The docking analysis suggests that zafirlukast can bind favorably to the RdRp receptor through a combination of extensive hydrogen bonding and electrostatic interactions. These findings warrant further investigation through *in vitro* and *in vivo* studies to assess the biological significance of this interaction.
Mizolastine binds to RdRp with a binding energy of -7.6 kcal/mol, indicating a relatively strong interaction (Table 5). This interaction involves various types of non-covalent forces, including hydrogen bonds, halogen bonds, and hydrophobic interactions. Hydrogen bond interactions occurs between 1,3-diazinan-2-yl group with Trp617 and Ala762 residues within distance of 3.79 Å and 6.58 Å, respectively. Additionally, the closest interaction, with a bond distance of 2.14 Å was observed between carbonyl and Ser814 residues. Also, pi-cation interaction of fluorophenyl and Arg553 aminoacid was detected at a distance of 4.74 Å. While the fluoro atom was detected at a distance that could form a halogen bond with the Asp623 residue, many hydrophobic interactions were observed with Tyr619, Pro620 and Lys621 residues.

Rupatadine interacts with RdRp with a binding energy of -7.2 kcal/mol, signifying a relatively strong binding affinity. The significant carbon hydrogen bonds, hydrophobic and electrostatic interactions were detected between rupatadine with key residues that Lys619, Lys621, Asp761, and Trp800 (Table 6). Hydrogen bond interaction occurred between the 5-methyl pyridine ring of Rupatadine and the Lys621 residue of RdRp. Rupatadine's 8-methyl-benzocyclohepta pyridine ring exhibited pi-anion interactions with Asp761 on RdRp. Also, two types of hydrophobic interactions are seen. One occurs between the (5-methylpyridin-3-yl)methyl group of rupatadine and the Tyr619 residue of RdRp. Another hydrophobic interaction involves the 8-methyl-benzocyclohepta pyridine ring of rupatadine and the Trp800 residue of RdRp.
Terfenadine interacts with RdRp with a binding energy of -7.1 kcal/mol, indicating a moderately strong interaction. This interaction involves various non-covalent forces, including hydrogen bonds, electrostatic interactions, and a carbon hydrogen bond (Table 7). An alcohol group on terfenadine forms a hydrogen bond with Asp760 residue of RdRp at distance of 2.17 Å. While the phenyl ring of terfenadine interacts with Asp618 of RdRp through electrostatic/pi-anion interactions, another electrostatic interaction occurs between another phenyl ring of terfenadine and Asp761 of RdRp.
The findings revealed that all seven-candidate drugs exhibited superior binding energies to RdRp compared to molnupiravir, its hydrolyzed form N-hydroxycytidine (NHC), and its mono-phosphorylated (NHC-MP) derivative. This translates to a potentially stronger affinity between the drugs and the enzyme, which could be crucial for disrupting viral replication. These findings not only deepen our understanding of the ligand-receptor interactions but also offer valuable guidance for rational drug design and optimization strategies aimed at developing effective antiviral therapeutics targeting RdRp.

DISCUSSION

The compounds with best binding energy and poses were bilastine, fexofenadine, montelukast, zafirlukast, mizolastine, rupatadine and terfenadine, respectively -7.6, -8.0, -7.2, -8.3, -7.6, -7.6 and -7.1 kcal/mol. All of these results are better than those of a previous study reported in 2021, which reported the binding energies of molnupiravir, its hydrolyzed form (NHC), and its mono-phosphorylated derivative (NHC-MP) as -5.7, -6.0, and -6.3 kcal/mol, respectively [34]. The higher target specificity and unique interactions of our compounds contribute to the stronger binding. Extensive validation and comparison with computational data further support our findings, suggesting these compounds may offer potential therapeutic benefits.
The binding energies of azelastine, buclizine, cyproheptadine, ebastine and loratadine were determined to be in the range of -6.9 to -6.6 kcal/mol and have better binding scores compared to molnupiravir. Cetirizine, desloratadine, hydroxyzine, levocetirizine, ketotifen, meclizine and olopatadine exhibited similar binding scores with molnupiravir (Figures 3-5). Moreover, it was found remarkable that the selected seven H1-antihistamines exhibited strong non-covalent interactions with amino acids Asp760 and Arg553, similar to molnupiravir and its derivatives (Figure 6).
The findings revealed that all seven-candidate drugs exhibited superior binding energies to RdRp compared to molnupiravir, its hydrolyzed form (NHC), and its mono-phosphorylated derivative (NHC-MP). This translates to a potentially stronger affinity between the drugs and the enzyme, which could be crucial for disrupting viral replication. These findings not only deepen our understanding of the ligand-receptor interactions but also offer valuable guidance for rational drug design and optimization strategies aimed at developing effective antiviral therapeutics targeting RdRp.
Antazoline, brompheniramine, carbinoxamine, chlorcyclizine, chlorpheniramine, clemastine, cyclizine, dexchlorpheniramine, dimenhydrinate, diphenhydramine, emedastine, promethazine, trimeprazine, tripelennamine,

uncorrected proof

and triprolidine all exhibited binding energies higher -5.7 kcal/mol. As a result, their findings were considered less significant compared to the other compounds discussed in this study. Therefore, we have excluded their conformational data from this analysis.

CONCLUSION

In conclusion, the docking study conducted in this research illuminates the intricate molecular interactions between montelukast, zafirlukast, fexofenadine, bilastine, mizolastine, rupatadine, terfenadine and the SARS-CoV-2 RdRp enzyme, shedding light on their potential as therapeutic agents against viral infections. Montelukast exhibited a binding profile characterized by hydrogen bonding, hydrophobic interactions, and electrostatic contacts with key residues of RdRp, highlighting specific molecular recognition patterns crucial for stabilizing the Montelukast-RdRp complex. Conversely, zafirlukast demonstrated a stronger binding affinity, engaging in an extensive network of hydrogen bonds involving multiple residues of RdRp, primarily mediated by carbamate and amide functional groups. Additionally, electrostatic interactions further contributed to the stability and specificity of the zafirlukast-RdRp complex. Moreover, the inclusion of fexofenadine, bilastine, mizolastine, rupatadine and terfenadine in the study offers insights into their potential interactions with RdRp, potentially expanding the repertoire of therapeutic options against RNA viruses. These findings provide valuable insights into the molecular mechanisms underlying the interactions between these ligands and RdRp, offering a foundation for further exploration of their antiviral potential and the development of novel therapeutic strategies targeting RNA viruses.

REFERENCES

[1] World Health Organization. Infectious diseases. Available at: https://www.emro.who.int/health-topics/infectious-diseases/index.html. Accessed May 25, 2024.
[2] McCarthy MK, Morrison TE. Persistent RNA virus infections: do PAMPS drive chronic disease? Curr Opin Virol. 2017;23:8-15.
[3] Lee M, Kim JW, Jang B. Dove: An infectious disease outbreak statistics visualization system. IEEE Access. 2018;6:47206-47216. doi:10.1109/ACCESS.2018.2867030.
[4] World Health Organization. Novel coronavirus disease (COVID-19) outbreak. Available at: https://www.who.int/emergencies/diseases/novel-coronavirus-2019. Accessed May 21, 2024.
[5] Zheng L, Zhang L, Huang J, Nandakumar KS, Liu S, Cheng K. Potential treatment methods targeting 2019-nCoV infection. Eur J Med Chem. 2020;205:112687. doi:10.1016/j.ejmech.2020.112687.
[6] Seliem IA, Panda SS, Girgis AS, Moatasim Y, Kandeil A, Mostafa A, Ali MA, Nossier ES, Rasslan F, Srour AM, Sakhuja R, Ibrahim TS, Abdel-samii ZKM, Al-Mahmoudy AMM. New quinoline-triazole conjugates: synthesis, and antiviral properties against SARS-CoV-2. Bioorg Chem. 2021;114:105117. doi:10.1016/j.bioorg.2021.105117.
[7] Zhou P, Yang XL, Wang XG, Hu B, Zhang L, Zhang W, Si HR, Zhu Y, Li B, Huang CL, Chen HD, Chen J, Luo Y, Guo H, Jiang RD, Liu MQ, Chen Y, Shen XR, Wang X, Zheng XS, Zhao K, Chen QJ, Deng F, Liu LL, Yan B, Zhan FX, Wang YY, Xiao GF, Shi ZL. A pneumonia outbreak associated with a new coronavirus of probable bat origin. Nature. 2020;579:270-273. doi:10.1038/s41586-020-2012-7.
[8] Krause R, Smolle J. Covid-19 mortality and local burden of infectious diseases: a worldwide country-by-country analysis. J Infect Public Health. 2022;15:1370-1375. doi:10.1016/j.jiph.2022.10.018.
[9] Drayman N, Jones KA, Azizi SA, Froggatt HM, Tan K, Maltseva NI, Chen S, Nicolaescu V, Dvorkin S, Furlong K, Kathayat RS, Firpo MR, Mastrodomenico V, Bruce EA, Schmidt MM, Jedrzejczak R, Muñoz-Alía MÁ, Schuster B, Nair V, Botten JW, Brooke CB, Baker SC, Mounce BC, Heaton NS, Dickinson BC, Jaochimiak A, Randall G, Tay S. Drug repurposing screen identifies masitinib as a 3CLpro inhibitor that blocks replication of SARS-CoV-2 in vitro. bioRxiv [Preprint]. 2020 Sep 1:2020.08.31.274639. doi:10.1101/2020.08.31.274639.
[10] Piplani S, Singh P, Winkler DA, Petrovsky N. Potential COVID-19 Therapies from Computational Repurposing of Drugs and Natural Products against the SARS-CoV-2 Helicase. Int J Mol Sci. 2022;23(14):7704. doi:10.3390/ijms23147704.
[11] Ghahremanpour MM, Tirado-Rives J, Deshmukh M, Ippolito JA, Zhang CH, Cabeza de Vaca I, Liosi ME, Anderson KS, Jorgensen WL. Identification of 14 Known Drugs as Inhibitors of the Main Protease of SARS-CoV-2. ACS Med Chem Lett. 2020;11(12):2526-2533. doi:10.1021/acsmedchemlett.0c00521.
[12] Reznikov LR, Norris MH, Vashisht R, Bluhm AP, Li D, Liao YSJ, Brown A, Butte AJ, Ostrov DA. Identification of antiviral antihistamines for COVID-19 repurposing. Biochem Biophys Res Commun. 2021;538:173-179. doi:10.1016/j.bbrc.2020.11.095.
[13] Oh KK, Adnan M, Cho DH. Network Pharmacology Study to Elucidate the Key Targets of Underlying Antihistamines against COVID-19. Curr Issues Mol Biol. 2022;44(4):1597-1609. doi:10.3390/cimb44040109.

uncorrected proof

[14] Liu J, Cao R, Xu M, Wang X, Zhang H, Hu H, Li Y, Hu Z, Zhong W, Wang M. Hydroxychloroquine, a less toxic derivative of chloroquine, is effective in inhibiting SARS-CoV-2 infection in vitro. Cell Discov. 2020;6:16. doi:10.1038/s41421-020-0156-0.
[15] Wang M, Cao R, Zhang L, Yang X, Liu J, Xu M, Shi Z, Hu Z, Zhong W, Xiao G. Remdesivir and chloroquine effectively inhibit the recently emerged novel coronavirus (2019-nCoV) in vitro. Cell Res. 2020;30:269-271. doi:10.1038/s41422-020-0282-0.
[16] Dyall J, Gross R, Kindrachuk J, et al. Middle East Respiratory Syndrome and Severe Acute Respiratory Syndrome: Current Therapeutic Options and Potential Targets for Novel Therapies. Drugs. 2017;77:1935-1966. doi:10.1007/s40265-017-0830-1.
[17] Simons F, Estelle R. Advances in H1-Antihistamines. N Engl J Med. 2004;351(21):2203-2217. doi:10.1056/NEJMra033121.
[18] Church MK. Allergy, Histamine and Antihistamines. In: Hattori Y, Seifert R, eds. Histamine and Histamine Receptors in Health and Disease. Handbook of Experimental Pharmacology, vol 241. Springer, Cham; 2016. doi:10.1007/164_2016_85.
[19] Lidia M, Martina F, Mairene C, Sofía P, Loreto B, Juan Manuel L, Jordi B, Xavier F, Pablo G. Selective inhibition of hepatitis C virus infection by hydroxyzine and benztropine. Antimicrob Agents Chemother. 2014;58(6):3451-3460.
[20] Zongyi H, Adam R, Xin H, Christopher D, Derek J, Seung BP, Michael H, Noel S, D Eric A, Daniel CT, John RL, Juan CM, T Jake L. Chlorcyclizine Inhibits Viral Fusion of Hepatitis C Virus Entry by Directly Targeting HCV Envelope Glycoprotein. Cell Chem Biol. 2020;27(6):780-792.
[21] Kitchen D, Decornez H, Furr J, et al. Docking and scoring in virtual screening for drug discovery: methods and applications. Nat Rev Drug Discov. 2004;3:935-949. doi:10.1038/nrd1549.
[22] Tian L, Qiang T, Liang C, Ren X, Jia M, Zhang J, Li J, Wan M, YuWen X, Li H, Cao W, Liu H. RNA-dependent RNA polymerase (RdRp) inhibitors: The current landscape and repurposing for the COVID-19 pandemic. Eur J Med Chem. 2021 Mar 5;213:113201. doi:10.1016/j.ejmech.2021.113201.
[23] de Farias ST, Dos Santos Junior AP, Rêgo TG, José MV. Origin and Evolution of RNA-Dependent RNA Polymerase. Front Genet. 2017 Sep 20;8:125. doi:10.3389/fgene.2017.00125. PMID: 28979293; PMCID: PMC5611760.
[24] Kirchdoerfer RN, Ward AB. Structure of the SARS-CoV nsp12 polymerase bound to nsp7 and nsp8 co-factors. Nat Commun. 2019 May 28;10(1):2342. doi:10.1038/s41467-019-10280-3. PMID: 31138817; PMCID: PMC6538669.
[25] Elfiky AA. Ribavirin, Remdesivir, Sofosbuvir, Galidesivir, and Tenofovir against SARS-CoV-2 RNA dependent RNA polymerase (RdRp): A molecular docking study. Life Sci. 2020 Jul 15;253:117592. doi:10.1016/j.lfs.2020.117592.
[26] Gao Y, Yan L, Huang Y, Liu F, Zhao Y, Cao L, Wang T, Sun Q, Ming Z, Zhang L, Ge J, Zheng L, Zhang Y, Wang H, Zhu Y, Zhu C, Hu T, Hua T, Zhang B, Yang X, Li J, Yang H, Liu Z, Xu W, Guddat LW, Wang Q, Lou Z, Rao Z. Structure of the RNA-dependent RNA polymerase from COVID-19 virus. Science. 2020 May 15;368(6492):779-782. doi:10.1126/science.abb7498.
[27] Hillen HS, Kokic G, Farnung L, Dienemann C, Tegunov D, Cramer P. Structure of replicating SARS-CoV-2 polymerase. Nature. 2020 Aug;584(7819):154-156. doi:10.1038/s41586-020-2368-8.
[28] Lung J, Lin YS, Yang YH, Chou YL, Shu LH, Cheng YC, Liu HT, Wu CY. The potential chemical structure of anti-SARS-CoV-2 RNA-dependent RNA polymerase. J Med Virol. 2020 Jun;92(6):693-697. doi:10.1002/jmv.25761.
[29] Choi J, Azmat CE. Leukotriene Receptor Antagonists. [Updated 2023 Jun 4]. In: StatPearls [Internet]. Treasure Island (FL): StatPearls Publishing; 2024 Jan-. Available from: https://www.ncbi.nlm.nih.gov/books/NBK554445/.
[30] Al Ghobain M, Rebh F, Saad A, Khan AH, Mehyar N, Mashhour A, Islam I, Alobaida Y, Alaskar AS, Boudjelal M, Al Jeraisy M. The efficacy of Zafirlukast as a SARS-CoV-2 helicase inhibitor in adult patients with moderate COVID-19 Pneumonia (pilot randomized clinical trial). J Infect Public Health. 2022 Dec;15(12):1546-1550. doi:10.1016/j.jiph.2022.11.016.
[31] Morris GM, Huey R, Lindstrom W, Sanner MF, Belew RK, Goodsell DS, Olson AJ. Software News and Updates Gabedit — A Graphical User Interface for Computational Chemistry Softwares. J Comput Chem. 2009;30:174–182.
[32] Stewart JJP. Optimization of parameters for semiempirical methods V: Modification of NDDO approximations and application to 70 elements. J Mol Model. 2007;13:1173–1213. doi:10.1007/s00894-007-0233-4.
[33] Trott O, Olson AJ. AutoDock Vina: improving the speed and accuracy of docking with a new scoring function, efficient optimization, and multithreading. J Comput Chem. 2010 Jan 30;31(2):455-61. doi:10.1002/jcc.21334.

uncorrected proof

[34] Kulabaş N, Yeşil T, Küçükgüzel İ. Evaluation of molnupiravir analogues as novel coronavirus (SARS-CoV-2) RNA-dependent RNA polymerase (RdRp) inhibitors – an in silico docking and ADMET simulation study. J Res Pharm. 2021;25(6):967-981.

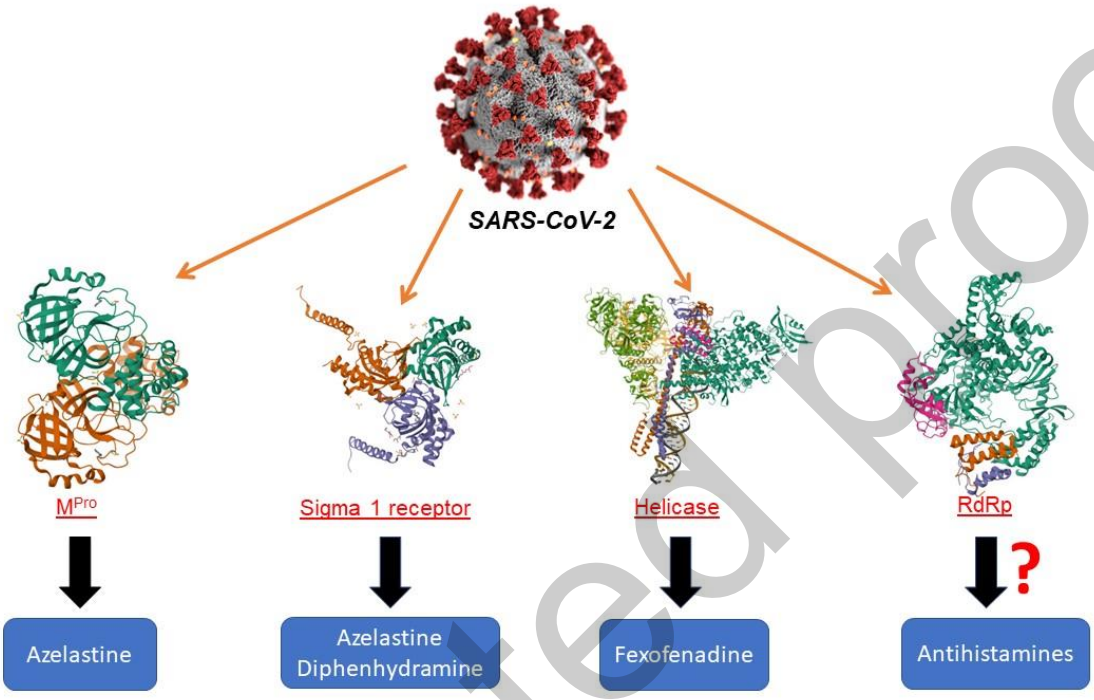

Figure 1. Antiviral effects of the known antihistamines against SARS-CoV-2

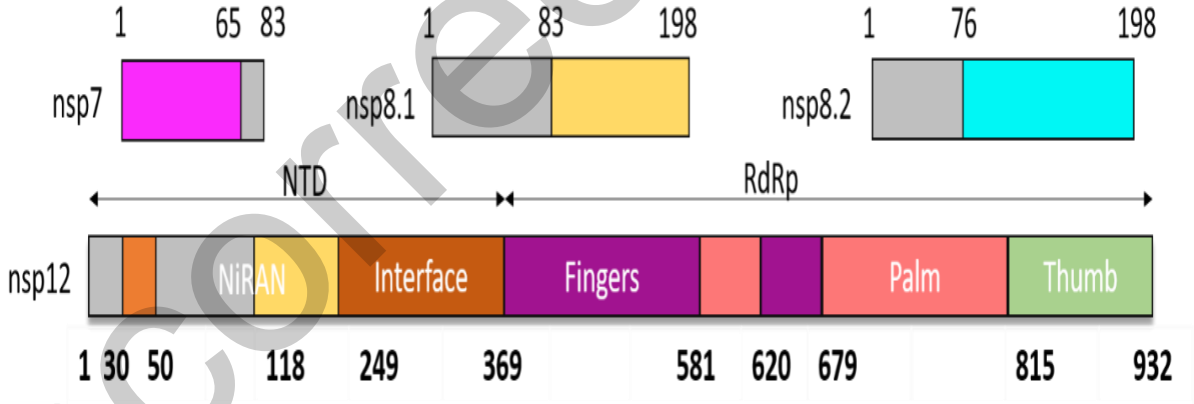

Figure 2. Domain organization of SARS-CoV-2 and its (RdRp). Interdomain boundaries are labeled with residue numbers. Here we can see Nsp12. RdRp: RNA-dependent RNA polymerase [22]

uncorrected proof

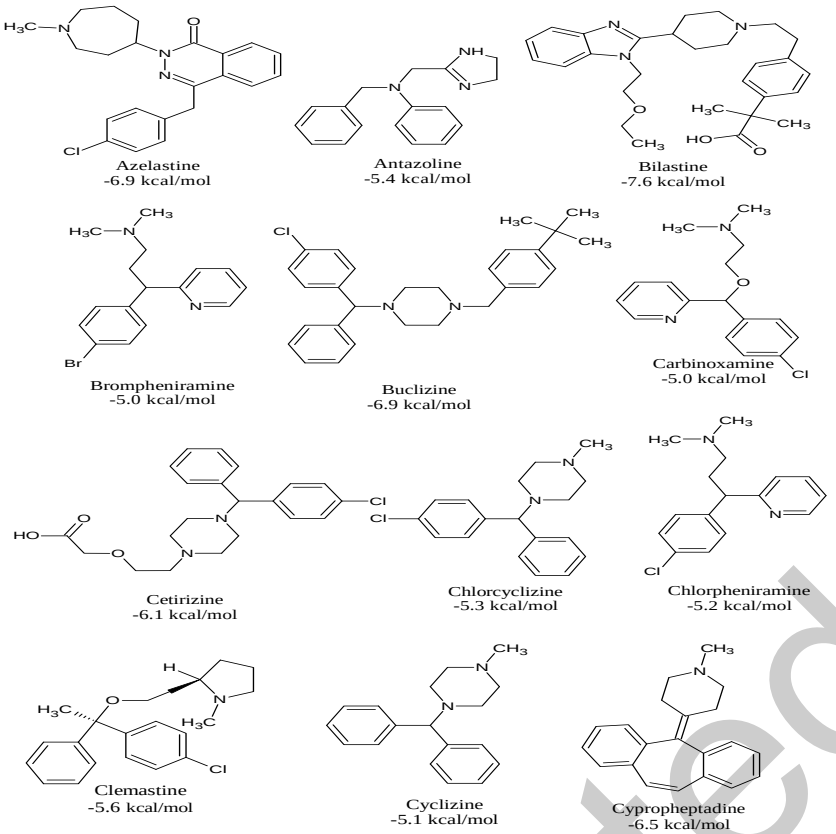

Figure 3: Binding energies of analyzed drugs to SARS-CoV-2 RdRp enzyme

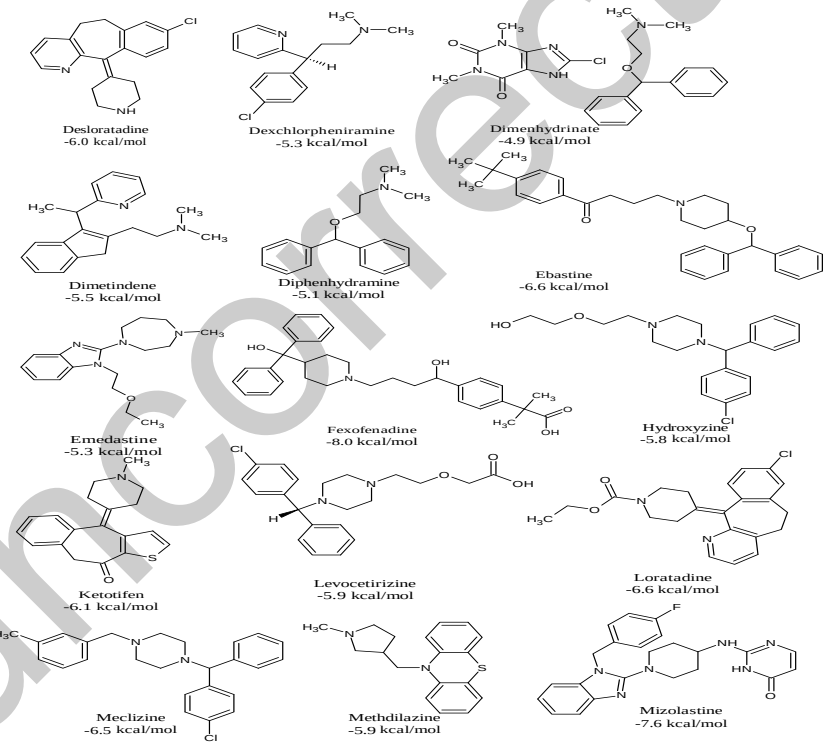

Figure 4: Binding energies of analyzed drugs to SARS-CoV-2 RdRp enzyme

uncorrected proof

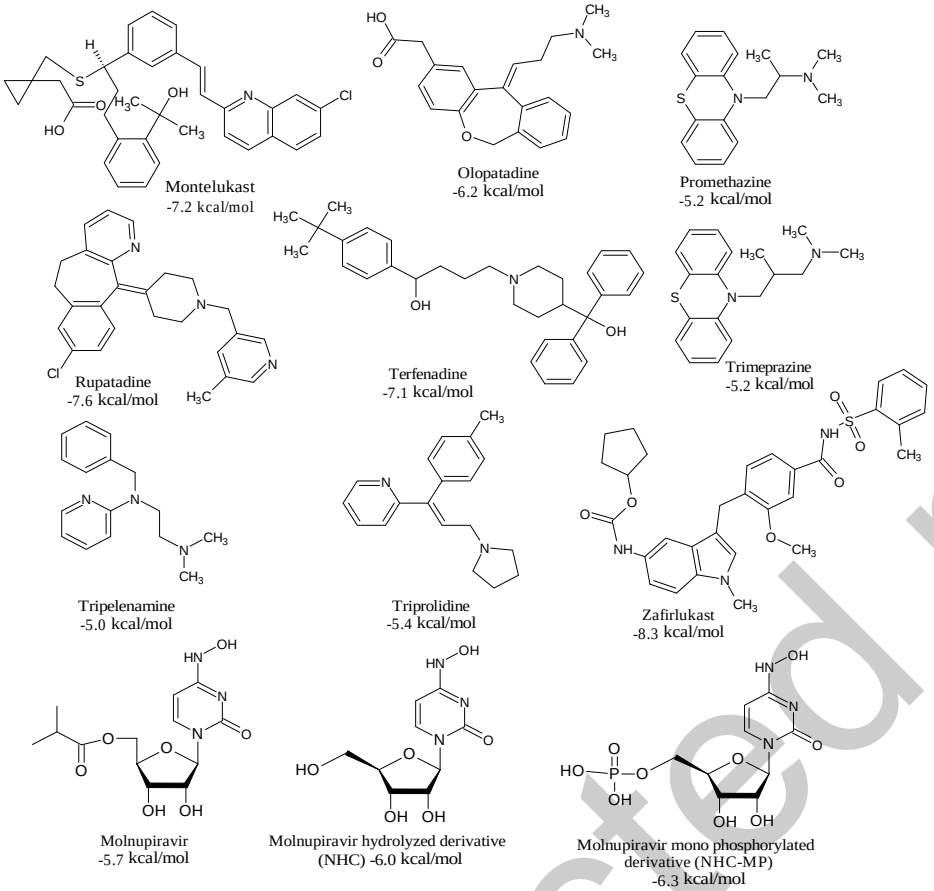

Figure 5: Binding energies of analyzed drugs to SARS-CoV-2 RdRp enzyme

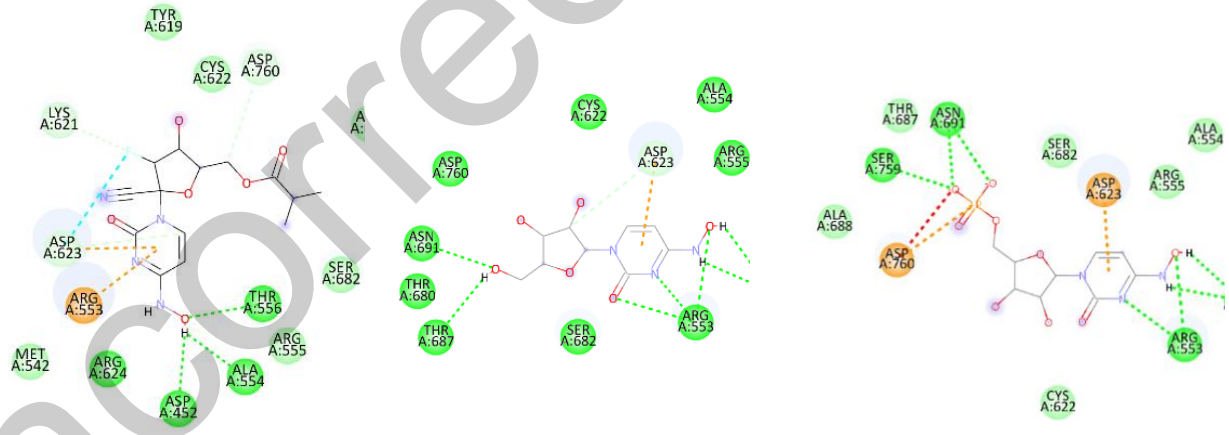

Molnupiravir

Hydrolyzed form of molnupiravir (NHC)

Mono-phosphorylated derivative of molnupiravir (NHC-MP)

Figure 6. Molnupiravir and its derivatives in SARS-CoV-2 RdRp active site

uncorrected proof

Table 1. Interactions of bilastine with the active site of RdRp.

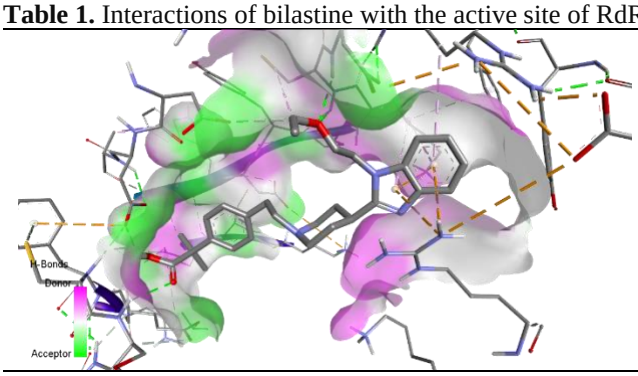

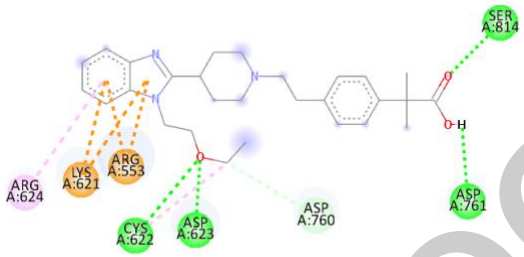

Functional Group	Residue	Bond	Distance (Å)
Carboxylic acid	Asp761	H-bond (A-B)	2.26
Carboxylic acid	Ser814	H-bond (D-B)	2.43
Ethoxy	Asp623	H-bond (D-S)	2.25
Ethoxy	Cyc622	H-bond (D-S)	2.27
Benzimidazole	Arg553	Electrostatic/pi- cation	4.27
Benzimidazole	Arg553	Electrostatic/pi- cation	4.32
Benzimidazole	Lys621	Electrostatic/pi- cation	4.94
Benzimidazole	Lys621	Electrostatic/pi-cation	4.78
Benzimidazole	Arg624	Hydrophobic/pi-alkyl	5.34
Ethoxy	Asp760	Carbon hydrogen bond	3.49
Ethoxy	Cys622	Hydrophobic/alkyl-alkyl	3.82

* Light green - Carbon hydrogen bond; Green - H-bond; Orange - Electrostatic interactions; Pink – Hydrophobic interactions.
* For amino acid, A:H-bond acceptor; D: H-bond donor; B: Backbone interaction; S: Sidechain interaction.

Table 2. Interactions of fexofenadine with the active site of RdRp.

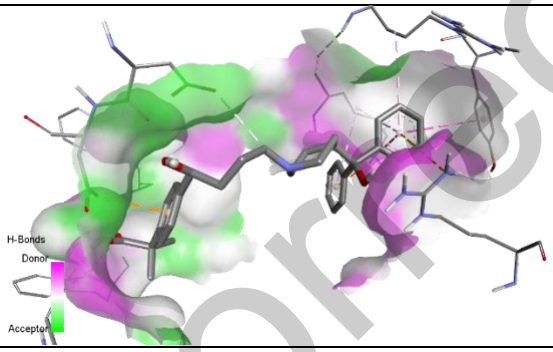

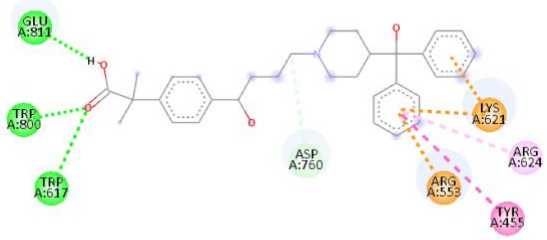

Functional Group	Residue	Bond	Distance (Å)
Carboxylic acid	Trp617	H-bond (D-S)	2.91
Carboxylic acid	Trp800	H-bond (D-B)	2.76
Carboxylic acid	Glu811	H-bond (A-B)	2.02
'Phenyl	Tyr455	Hydrophobic/Pi-Pi T-form	5.57
'Phenyl	Arg553	Electrostatic/pi-cation	4.38
'Phenyl	Lys621	Electrostatic/pi-cation	4.62
'Phenyl	Arg624	Hydrophobic/pi-alkyl	3.09
"Phenyl	Lys621	Electrostatic/pi-cation	5.46
Butyl	Asp760	Carbon hydrogen bond	3.59

* Light green - Carbon hydrogen bond; Green - H-bond; Orange - Electrostatic interactions; Pink – Hydrophobic interactions.
* For aminoacid, A:H-bond acceptor; D: H-bond donor; B: Backbone interaction; S: Sidechain interaction.

uncorrected proof

Table 3. Interactions of Montelukast with the active site of RdRp.

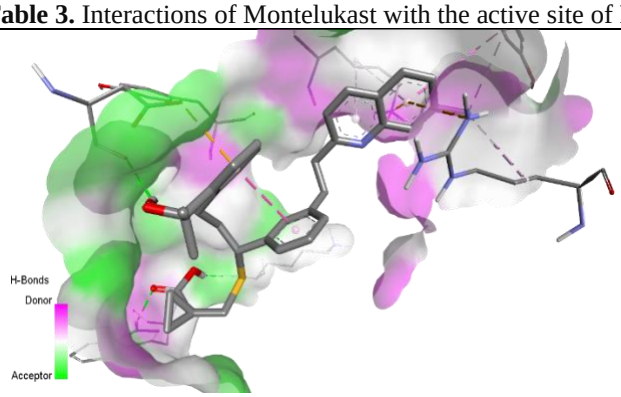

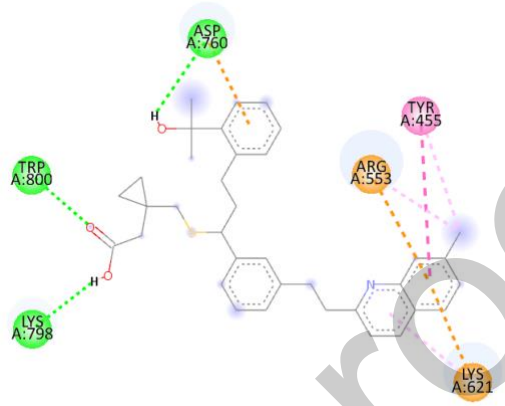

Functional Group	Residue	Bond	Distance (Å)
2-Hydroxypropan-2-yl	Asp760	H-bond (A-S)	2.73
Carboxylic acid -COOH	Lys798	H-bond (A-S)	2.20
Carboxylic acid -COOH	Trp800	H-bond (D-B)	2.10
7-Methylquinoline	Tyr455	Hydrophobic/pi-alkyl	4.19
7-Methylquinoline	Tyr455	Hydrophobic/Pi-Pi T-form	5.85
7-Methylquinoline	Arg553	Hydrophobic/alkyl-alkyl	4.39
7-Methylquinoline	Arg553	Electrostatic/pi-cation	4.42
7-Methylquinoline	Lys621	Electrostatic/pi-cation	4.13
7-Methylquinoline	Lys621	Hydrophobic/pi-alkyl	4.50
4-(2-Hydroxypropan-2-yl)phenyl	Asp760	Electrostatic/Pi-anion	3.25

* Green - H-bond; Orange - Electrostatic interactions; Pink – Hydrophobic interactions.
* For aminoacid, A:H-bond acceptor; D: H-bond donor; B: Backbone interaction; S: Sidechain interaction.

Table 4. Interactions of zafirlukast with the active site of RdRp.

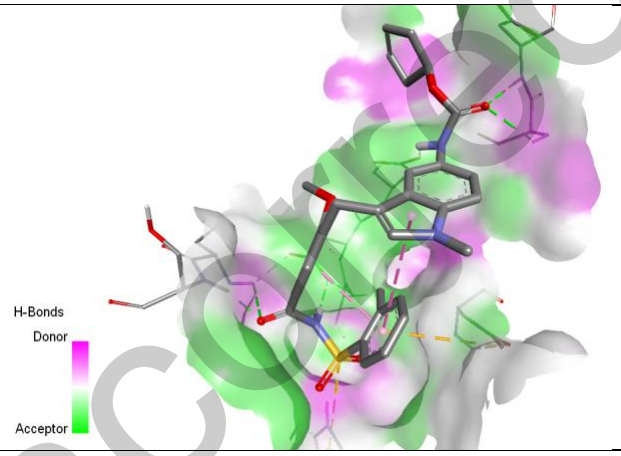

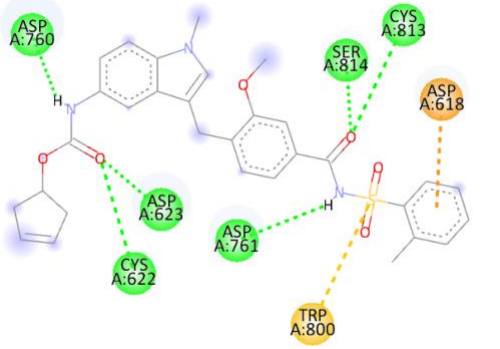

Functional Group	Residue	Bond	Distance (Å)
Carbamate-NHCOO-	Cys622	H-bond (D-S)	2.61
Carbamate-NHCOO-	Asp623	H-bond (D-S)	2.24
Carbamate-NHCOO-	Asp760	H-bond (A-B)	2.29
Amide-CONH-	Asp761	H-bond (A-B)	2.06
Amide-CONH-	Cys813	H-bond (D-S)	2.91
Amide-CONH-	Ser814	H-bond (D-S)	1.83
Benzene Sulfonyl	Asp618	Electrostatic/pi-anion	4.65
Benzene Sulfonyl	Trp800	Pi-sulfur	4.84

* Green - H-bond; Orange - Electrostatic interactions.
* For aminoacid, A:H-bond acceptor; D: H-bond donor; B: Backbone interaction; S: Sidechain interaction.

uncorrected proof

Table 5. Interactions of mizolastine with the active site of RdRp.

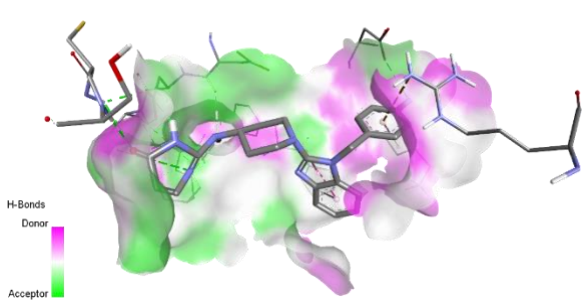

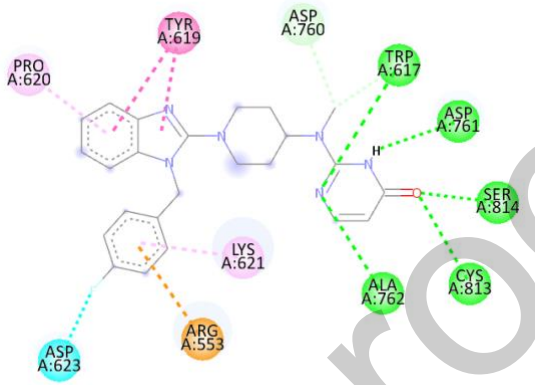

Functional Group	Residue	Bond	Distance (Å)
1,3-Diazinan-2-yl	Trp617	H-bond (D-S)	3.79
1,3-Diazinan-2-yl	Ala762	H-bond (D-S)	6.58
Carbonyl	Ser814	H-bond (D-S)	2.14
Carbonyl	Gln815	H-bond (D-S)	5.74
N-methyl	Trp617	Carbon hydrogen bond	3.60
N-methyl	Asp760	Carbon hydrogen bond	3.26
Fluorophenyl	Arg553	Electrostatic/pi-cation	4.74
Fluorophenyl	Lys621	Hydrophobic/pi-alkyl	5.04
Fluorophenyl	Asp623	Halogen bond	3.15
Benzimidazole	Pro620	Hydrophobic/pi-alkyl	4.90
Benzimidazole	Tyr619	Hydrophobic/Pi-Pi T-form	4.82
Benzimidazole	Tyr619	Hydrophobic/Pi-Pi T-form	4.86

*Light green- Carbon H-bond; Green- H-bond; Orange- Electrostatic interaction; Pink– Hydrophobic interaction; Blue- Halogen bond.
*For aminoacid, A:H-bond acceptor; D: H-bond donor; B: Backbone interaction; S: Sidechain interaction.

Table 6. Interactions of rupatadine with the active site of RdRp.

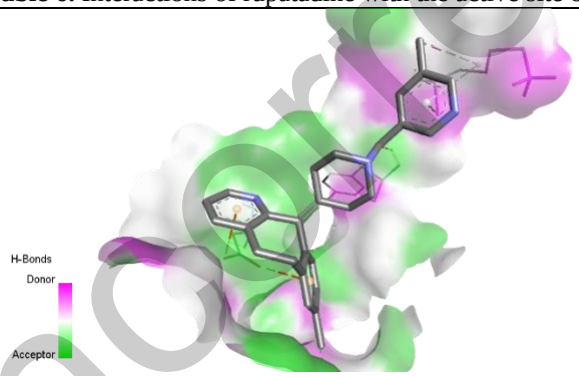

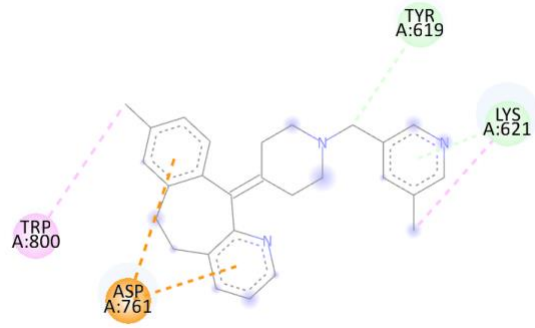

Functional Group	Residue	Bond	Distance (Å)
5-MethylPyridine	Lys621	Carbon hydrogen bond	2.89
5-MethylPyridine	Lys621	Hydrophobic/alkyl-alkyl	4.17
(5-MethylPyridin-3-yl)methyl	Tyr619	Carbon hydrogen bond	3.51
8-methyl-BenzocycloheptaPyridine	Asp761	Electrostatic/Pi-anion	3.30
8-methyl-BenzocycloheptaPyridine	Asp761	Electrostatic/Pi-anion	3.95
8-methyl-BenzocycloheptaPyridine	Trp800	Hydrophobic/pi-alkyl	4.33

* Light green - Carbon H-bond; Orange - Electrostatic interactions; Pink – Hydrophobic interactions.

uncorrected proof

Table 7. Interactions of terfenadine with the active site of RdRp.

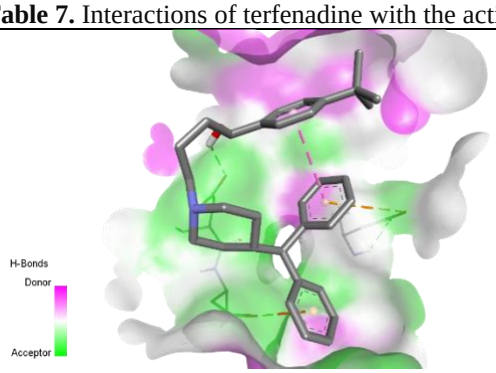

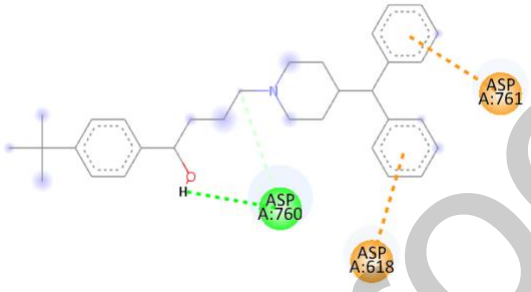

Functional Group	Residue	Bond	Distance (Å)
Alcohol	Asp760	H-bond (D-B)	2.17
'Phenyl	Asp618	Electrostatic/Pi-anion	4.62
Butyl	Asp760	Carbon hydrogen bond	3.54
"Phenyl	Asp761	Electrostatic/Pi-anion	3.59

* Light green - Carbon H-bond; Green - H-bond; Orange - Electrostatic interactions.
* For aminoacid, A:H-bond acceptor; D: H-bond donor; B: Backbone interaction; S: Sidechain interaction.

uncorrected proof